Antiferromagnetic V_2O_3 based exchange coupling

Ralph el Hage,[1] Tianxing D. Wang,[1,2] Junjie Li,[1,2] Ali C. Basaran,[1] Felipe Torres,[3,4] and Ivan K. Schuller[1]
[1]*Department of Physics and Center for Advanced Nanoscience, University of California San Diego, La Jolla, California 92093, USA*
[2]*Materials Science and Engineering Program, University of California San Diego, La Jolla, California 92093, USA*
[3]*Department of Physics, Universidad de Chile, Santiago 7800024, Chile*
[4]*Center for the Development of Nanoscience and Nanotechnology, CEDENNA, Santiago 9170124, Chile*

(Received 5 August 2023; revised 25 March 2024; accepted 23 April 2024; published 13 May 2024)

Vanadium sesquioxide (V_2O_3) is a strongly correlated electronic material that famously undergoes a triple coupled first-order transition where it transitions from a paramagnetic metal with a rhombohedral structure at high temperature to an antiferromagnetic insulator with a monoclinic structure. While several studies have used one of both electronic and structural transitions to control the properties of a heterostructure, evidence of magnetic coupling has notoriously yet to be found. In this paper, we report on a robust magnetic coupling between the antiferromagnetic (AFM) V_2O_3 and ferromagnetic (FM) Permalloy (Py) layers that results in a significant exchange bias and strain-induced coercivity enhancement. We provide a temperature and angle-dependent study of magnetic properties, which clearly indicates exchange bias at the AFM/FM interface that appears at the onset of the metal-insulator transition. The magnitude of the exchange bias is strongest when the field is applied along the [001] V_2O_3 crystallographic orientation which corresponds to an AFM spin configuration on the [110] surface. This opens the door to designing and implementing novel functionalities in transition metal oxide-based computing using the connection between magnetism and the metal-insulator transition.

DOI: 10.1103/PhysRevMaterials.8.054407

I. INTRODUCTION

The study of interface effects in magnetism has been the subject of intense research in past decades ranging from the discovery of emergent phenomena [1] to potential uses in technological applications. Chief amongst them is the exchange bias (EB) [2] occurring between a ferromagnetic (FM) and an antiferromagnetic layer (AFM), which appears as a shift of the FM hysteresis loop away from zero fields. When FM layers are combined with antiferromagnetic functional materials, improved functionalities arise by adding additional magnetic degrees of freedom. This effect has been exploited to reduce power consumption in numerous commercially available devices such as magnetoresistive random-access memory, magnetic sensors [3], spin valves [4], and spintronic devices [5].

Vanadium sesquioxide (V_2O_3) is a strongly correlated electronic material that famously undergoes a triple coupled first-order transition where it transitions from a paramagnetic metal with a rhombohedral structure at high temperature to an antiferromagnetic insulator with a monoclinic structure. When V_2O_3 is coupled to a FM layer, it can act as an active component enhancing coercivity through strain [6,7], shunting due to insulator to metal transition (IMT) in a nanoconstriction [8], controlling a spin valve [9], or as an active layer in spin-orbit torque devices [10]. The combination of functional layers in artificially layered heterostructure including one or more transition metal oxides has allowed control of the magnetic [11], optical [12], and electrical [13,14] properties of devices. Interestingly, the interactions stemming from the magnetic coupling between the AFM phase of V_2O_3 and a FM layer in a heterostructure, i.e., exchange bias, have remained elusive for a long time, although some recent reports have claimed an appearance of a relatively weak coupling [15,16].

The coupled magnetic, electronic, and structural properties across the V_2O_3 transition can not only be triggered by temperature but also by electric field, strain, and local heat [17–19]. These additional switching methods of the V_2O_3 transition provide the potential for multifunctional applications such as in neuromorphic computing and spintronics [19]. Hence, a V_2O_3 based EB system can provide functionalities beyond those of a classical exchange biased AFM/FM heterostructure.

Here, we report on a robust magnetic coupling between the V_2O_3 and Py in heterostructures. This results in a significant exchange bias and strain-induced coercivity enhancement caused by the V_2O_3 magnetic and structural phase transitions. We provide a temperature and angle-dependent study of magnetic properties, which clearly indicates exchange bias at the interface between AFM V_2O_3 and an FM layer. The angular study also shines light on the AFM spin configuration of the V_2O_3 at the interface and paves the way to develop devices that use this coupling.

II. METHODS AND EXPERIMENT

V_2O_3 films were grown by reactive radio frequency (rf) magnetron sputtering on [110] oriented Al_2O_3 substrates (*A* cut). The Al_2O_3 substrates were prepared using an ultrasonic cleaner with acetone and methanol solution separately, each with a 10-min duration. Then, the substrate was thoroughly washed with isopropyl solution and dried with ultrahigh purity nitrogen gas to clean off residual contamination. The samples

 ©2024 American Physical Society

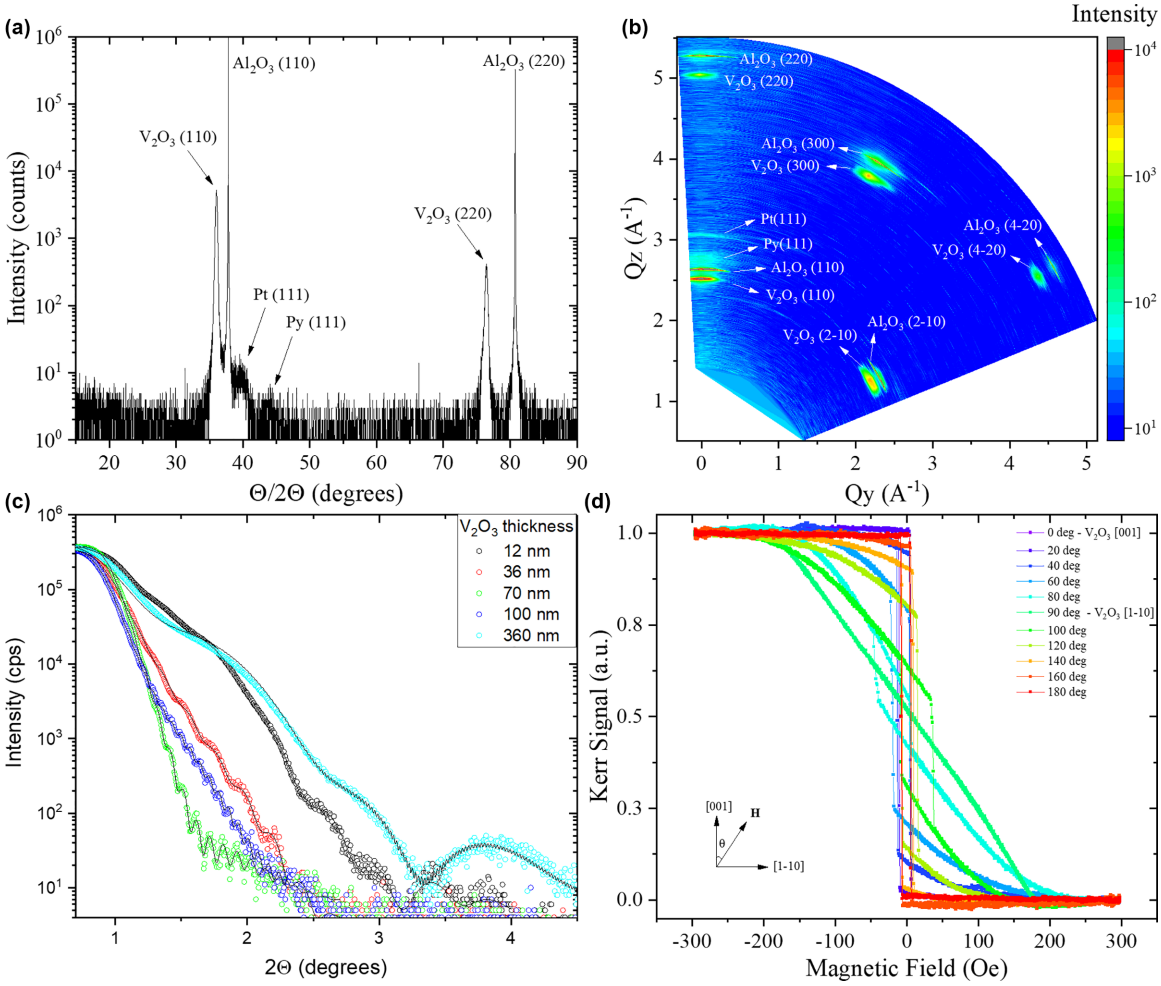

FIG. 1. Uniaxial anisotropic Py on *a*-cut V_2O_3. (a) X-ray diffraction (XRD) scan of an Al_2O_3/V_2O_3/Py/Pt heterostructure in specular geometry. The different peaks have been indexed. (b) Wide range reciprocal space map obtained by a Chi rotation of the sample showing pairs of Al_2O_3 and V_2O_3 peaks. (c) X-ray reflectivity measurements and fitting of samples with varying V_2O_3 thicknesses. (d) In-plane MOKE loops for different applied in-plane field angles. 0° and 90° indicate the applied field along the V_2O_3 [001]/[1–10] crystallographic directions, respectively. The inset shows the measurement geometry. These MOKE loops were measured at room temperature before FC.

were grown in a 7.9-mTorr Ar atmosphere and at a substrate temperature of 640 °C from a homemade V_2O_3 sputter target at a rate of ∼1.6 Å/s. After the growth, the samples were thermally quenched at a rate of ∼ 90 °C min^{-1}. This step has been shown to drastically improve the film's electronic properties [20]. Without breaking the vacuum, a 5-nm permalloy (Py) layer is then deposited from a commercial Py sputter target by rf sputtering in a 3-mTorr Ar atmosphere at a rate of 1 Å/s. A Pt capping layer is then deposited by DC sputtering to prevent the oxidation of the Py surface and unwanted changes in the sample stoichiometry.

Magneto-optical Kerr effect measurements were performed in a Montana Instruments NanoMOKE 3 system. The light source was a 660-nm laser focused on an approximately 5-μm spot. The magnetic field was cycled at a 0.13-Hz repetition rate. The sample was mounted on a stage in a closed cycle refrigerator cryostat with optical windows. Additional magnetic moment versus temperature curves were measured using a Quantum Design Dynacool system with the vibrating sample magnetometer (VSM) module. The vibrating frequency was set to 40 Hz and the amplitude to 2 mm. The samples were attached to a quartz sample holder using rubber cement. Angular adjustments of the sample were made manually using a protractor. The temperature was cycled between 50 and 220 K at a 2-K/min rate. X-ray diffraction measurements were performed in a Rigaku SMARTLAB diffractometer using Cu *K*-alpha radiation and a five-axis goniometer. Thickness and roughness parameters were extracted from x-ray reflectivity fitting using the GENX 3.6 software package [21].

III. MAIN RESULT

We have grown several V_2O_3 thin films under similar growth conditions on different crystallographic orientations of sapphire substrates. The V_2O_3 along the [110] direction maximizes the coupling between AFM spins at the V_2O_3 surface and the FM layer resulting in a significant exchange bias. Fig. 1 shows the x-ray diffraction spectra of a V_2O_3/Py/Pt heterostructure measured in the specular geometry. The appearance of both the [110] V_2O_3 and the [110] Al_2O_3 peaks

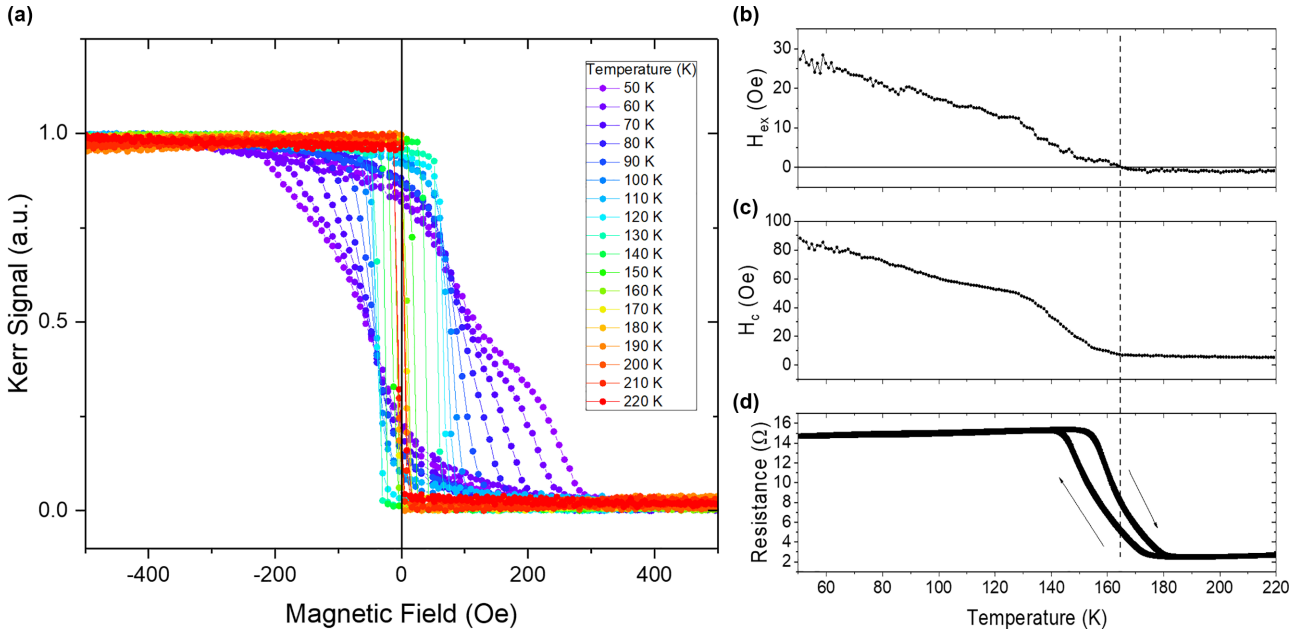

FIG. 2. Exchange bias and enhancement of coercivity. (a) In-plane MOKE loops measured on an Al_2O_3/V_2O_3/Py/Pt heterostructure while increasing temperature after a 500 Oe field cooling (FC) along the V_2O_3 [001] crystallographic direction. (b) Temperature dependence of the exchange field H_{ex}, (c) the coercive field H_c, and (d) an in-plane four-probe resistance measurement. The dashed line indicates the V_2O_3 metal-to-insulator transition (MIT).

in specular geometry at 36.05° and 37.81° implies highly oriented growth of V_2O_3, as has been previously reported [20,22]. We also note the appearance of diffraction peaks at 2θ angles of 37.8° and 44°, indicating textured growth of the Py and Pt layers along the [111] direction, typical of these heterostructures [23]. Figure 1(b) shows a wide range reciprocal space map obtained by rotating the sample along an axis perpendicular to the x-ray beam (Chi rotation). Bragg peaks corresponding to both film and substrate confirm the highly textured growth of V_2O_3 on the Al_2O_3 substrate. Figure 1(c) shows x-ray reflectivity (XRR) scans (solid points) of several V_2O_3/Py heterostructures where we varied the thickness of the V_2O_3 layer between 12 and 360 nm as well as their respective fits (lines).

Figure 1(d) shows averaged magneto-optical Kerr effect (MOKE) loops showing the magnetization reversal of the Py layer measured on a V_2O_3 (120 nm)/Py (5 nm) at room temperature while varying the angle between the in-plane applied field and the sample by rotating the sample. The curves labeled 0 and 90° correspond to the field applied along the [001] and [1–10] V_2O_3 crystallographic direction, respectively. The curves labeled 0 and 180° (shown in red and purple) correspond to hysteresis loops typically obtained along an easy axis characterized by a sharp and single jump in the magnetization. On the other hand, the curve labeled 90° corresponds to one obtained along a hard axis exhibiting a gradual and continuous change in magnetization.

Figure 2 shows averaged MOKE loops obtained while increasing temperature after a −500-Oe field cooling on the same V_2O_3 (120 nm)/Py (5 nm) sample. The magnetic field is applied along the [001] V_2O_3 crystallographic direction in the sample plane. At high temperatures, the magnetization reversal is reminiscent of an easy-axis behavior where the magnetization reverses in a single and sharp jump for each branch. As the temperature decreases, however, the hysteresis loop widens, and the remnant magnetization starts decreasing as its general shape changes from squarelike to springlike. This change in shape suggests a difference in the magnetization reversal mechanism, where increasing pinning of FM magnetization takes place as the temperature decreases.

Figures 2(b) and 2(c) confirm the magnetic coupling change where the exchange bias field H_{ex} and coercive field H_c are plotted as a function of temperature. H_{ex} decreases from about 26 Oe at 50 K with increasing temperature, and vanishes around 165 K. On the other hand, H_c decreases significantly over the whole temperature range by close to an order of magnitude. The temperature at which H_{ex} appears and H_c starts increasing corresponds to the middle of the V_2O_3 metal-to-insulator transition (MIT), as shown by the temperature-dependent resistance measurement of the same sample. This is highlighted by the dotted line in Fig. 2(d). Note that the resistance is measured across the entire heterostructure, in which the Py and Pt layers dominate electrical conduction, as the temperature is swept across the V_2O_3 phase transition. This explains both the metallic behavior of the resistance above and below the MIT as well as the suppression of the absolute change in resistance attributed to the V_2O_3 MIT.

The appearance of a robust exchange bias in this sample is somewhat surprising since it was not observed before in our previous studies with V_2O_3/Ni systems [24,25]. To further investigate the dependence of the exchange bias observed in the V_2O_3/Py heterostructure, we varied the angle (θ) at which the field cooling was applied. We also studied the same sample in a separate vibrating sample magnetometry system. The magnetization reversal hysteresis loops measured by VSM at 50 K for the same field cooling

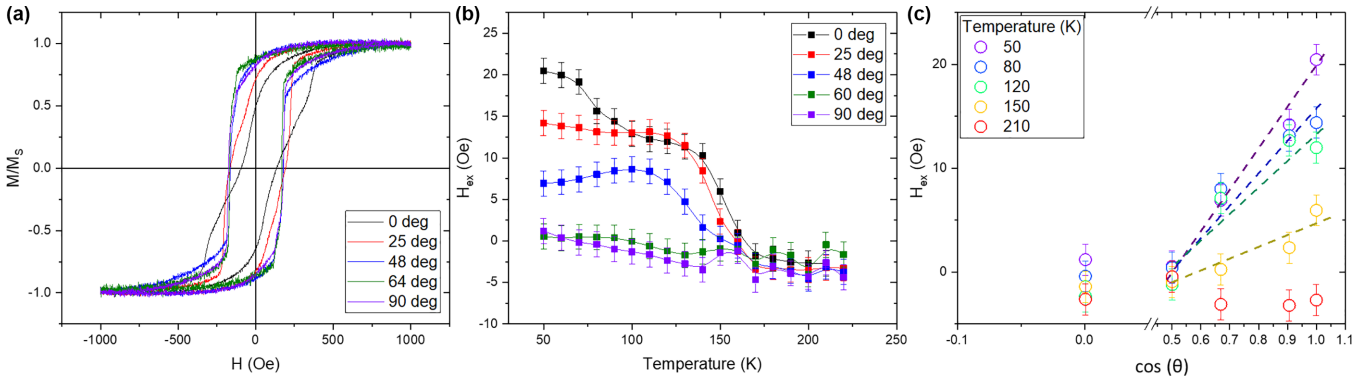

FIG. 3. Exchange bias dependence on field cooling angle. (a) Magnetization reversal hysteresis loops measured by VSM at 50 K for different field cooling directions. 0° and 90° indicate a field applied parallel to the V_2O_3 [001]/[10−1] crystallographic directions, respectively. (b) Temperature dependence of the exchange bias field H_{ex} for different field cooling directions. (c) Exchange bias field as a function of cos (θ) at various temperatures.

conditions applied at different angles are shown in Fig. 3(a). Aligning the external field to the V_2O_3 [001] and [1–10] crystallographic direction corresponds to $\theta = 0^\circ$ and $\theta = 90^\circ$, respectively. At 50 K, the shape of the hysteresis loop gradually changes as θ increases from 0 to 90°: with a hysteresis loop evolving from a springlike behavior that develops at low temperature when the field is along the [001] direction to a squarelike loop where the magnetization reversal happens abruptly when the field is applied along the [1–10]. Figure 3(b) shows the exchange bias field as a function of temperature for different applied field configurations for the same cooling protocols. Below the V_2O_3 Néel temperature and when the field is applied along the [001] direction the exchange bias field measured is highest and reaches close to 20 Oe at 50 K. As θ increases, a gradual decrease in the maximal exchange field is measured at 50 K until no exchange bias is found at $\theta = 60^\circ$. No exchange bias is observed when the external field is applied along the [1–10] crystallographic direction. The features around 100 K may result from changes in the coupling strength due to the decrease in thermal fluctuations at lower temperatures. The magnetic reversal also changes from a steplike to a springlike behavior at temperatures below 100 K [Fig. 2(a)]. The details are discussed in the next section. Figure 3(c) summarizes the angular behavior of the exchange bias observed on this sample at different temperatures. The cos(θ) dependence highlights the linear dependence of the unidirectional anisotropy energy term $K_{UD}\cos(\theta)$ in the macroscopic model.

Figure 4 shows MOKE loops obtained at 50 and 220 K on six different V_2O_3/Py samples where the thickness of the V_2O_3 layer varies from 12 to 360 nm after the same −500-Oe field cooling protocol. At 220 K, the magnetization reversal hysteresis loops are qualitatively similar for all six samples indicating minimal changes between the samples above the V_2O_3 AFM transition. On the other hand, the magnetic hysteresis loops at 50 K (below the AFM transition of V_2O_3) vary significantly between the samples. As the thickness of the V_2O_3 layer increases, the hysteresis loop shape evolves from a squarelike loop to a springlike loop [Figs. 4(g)–4(l)]. This hysteresis loop shape hints at a change in the magnetization reversal mechanism of the exchange coupled Py with increasing AFM V_2O_3 thickness, which could also be related to the interfacial properties.

IV. DISCUSSION

The FM layer grown on (110) V_2O_3 is characterized by an in-plane uniaxial anisotropy [Fig. 1(d)]. As the field direction is rotated by 90° in the sample plane, the magnetization reversal mechanism changes. This has been previously reported in the literature [16,23,25] and attributed to the microstructure of the film, i.e., the presence of rips and terraces on the V_2O_3 surface. This results in a strong domain wall pinning along one direction that can lead to a change in the magnetization reversal mechanism. Furthermore, the sudden increase in coercivity at the onset of the V_2O_3 MIT in Fig. 2(c) has also been observed in the literature [6] and attributed to structural phase coexistence as the vanadium oxide undergoes the phase transitions.

While V_2O_3/Ni and V_2O_3/Py bilayers share many similarities, the absence of EB in V_2O_3/Ni bilayer [24,25] may be due to the following reasons. First of all, Ni has a much larger magnetostriction than that of Py. The stress-induced uniaxial or biaxial anisotropy can dominate over any unidirectional anisotropy. In addition, Py has a smaller magnetocrystalline anisotropy which may facilitate AFM domain formation as field cooled across the triple V_2O_3 transition. Moreover, the V_2O_3/Ni bilayers in Refs. [24,25] are grown on *r*-cut sapphire while V_2O_3/Py bilayers are grown on *a*-cut sapphire substrates. The choice of substrate orientation can affect the morphology of the V_2O_3/Py interface and hence impacts on the magnetic coupling. All factors mentioned above are essential to the fact that EB can be observed in V_2O_3/Py but not in V_2O_3/Ni bilayers.

The exchange bias (EB) observed in V_2O_3/Py heterostructure is produced by the magnetic coupling between the AFM V_2O_3 and the ferromagnetic Py. This is indicated by the appearance of EB at the V_2O_3 AFM transition temperature, also indicated by the MIT [Fig. 2(c)]. The magnitude of the EB depends on the relative direction of the cooling field with respect to the V_2O_3 crystallographic direction, as plotted in Fig. 3(c). The highest exchange bias field is observed when the field cooling (FC) is applied along the V_2O_3 [001] crystallographic

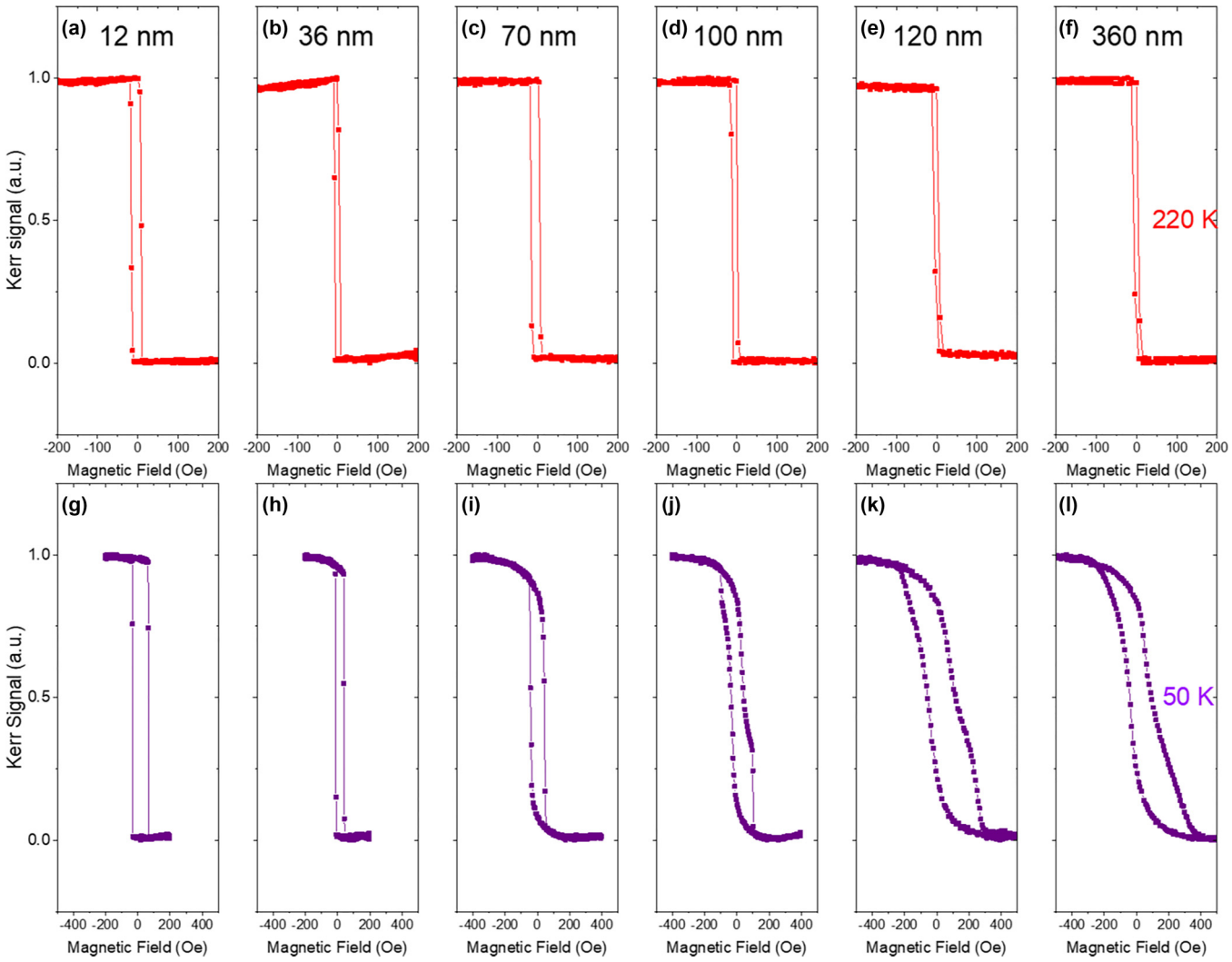

FIG. 4. Hysteresis loop evolution with AFM thickness in-plane MOKE loops of Al_2O_3/V_2O_3/Py/Pt heterostructure with varying V_2O_3 thicknesses as indicated on each top panels (a)–(f) at 220 K, and (g)–(l) at 50 K after a field cooling of −500 Oe along the V_2O_3 [001] crystallographic direction.

direction, the direction in which the spins are ferromagnetically aligned (see Fig. S1 of the Supplemental Material [26]). When the direction of the FC is applied at 60° with respect to the [001] direction, the magnitude of the exchange field is greatly diminished since neighboring vanadium atoms along this direction are antiferromagnetically aligned.

Although recent reports have demonstrated exchange bias in V_2O_3 based systems ([15,16]), these measurements have proven to be challenging. We attribute our positive findings to the following factors:

(1) The use of Py as an FM material with little magnetostriction. Vanadium sesquioxide undergoes a structural phase transition (from rhombohedral to monoclinic) coupled to its antiferromagnetic phase transition, which has a drastic effect on the properties of the exchange coupled neighboring FM, i.e., an increase in the coercive field at the antiferromagnetic transition which could effectively mask any exchange interaction on the properties of the FM layer.

(2) The orientation of the V_2O_3 layer at the interface. The AFM spin configuration is expected to consist of ferromagnetically aligned spins on V atoms in the (010) plane, with antiferromagnetic coupling between (010) planes [27,28]. The in-plane anisotropy and the V_2O_3 surface topography are expected to preferentially align FM spins along specific crystallographic orientations such as [001]. This would in turn lead to strong coupling along certain crystallographic directions such as [001] and result in a measurable exchange bias. A schematic representation of the antiferromagnetically aligned V_2O_3 spins at the interface along the [110] crystallographic orientation is illustrated in Fig. S1 [26].

(3) The relative size of the exchange bias effect (∼ 30% of the coercive field) depends strongly on the state of the AFM/FM interface. With the same magnetic protocol, the results are different if the vacuum is broken between the V_2O_3 and the Py growths. In this case, the exchange bias and the low temperature springlike loop are absent highlighting the importance of the interfacial coupling in these systems (Figs. S2c and S2d [26]).

The evolution of the magnetization reversal loops with the thickness of the AFM seen in Figs. 4(a)–4(l) is governed by the effective size of the magnetic domains in the V_2O_3 layer. The change in the qualitative shape of the

magnetization reversal loops is monotonous with $t_{V_2O_3}$ [Figs. 4(g)–4(l)]. Decreasing V_2O_3 thickness decreases the AFM grain and domain sizes. This produces a decrease in the effective pinning of the FM layer during magnetization reversal. See the Supplementary Material [26] for detailed discussion (see also Refs. [29–31] therein). This leads to the change in the shape of the hysteresis loop from a springlike to an abrupt squarelike behavior. The exchange spring can be observed not only in hard-soft FM configurations but also in EB systems [32]. It was predicted that for a compensated AFM interface, EB energy is mainly stored in the so-called incomplete domain wall (the twist of exchange spring) close to the interface in the FM layer [33]. In V_2O_3/Py, when the temperature goes below ∼100 K, the reversal behavior becomes springlike along the [001] orientation [Fig. 2(a)], and it is accompanied by a sizable increase of H_{ex} [Fig. 3(b)]. We speculate that decreased thermal fluctuations at lower temperatures allow for better pinning of the AFM layer close to the interface, hence enhancing the exchange spring region which reflects on the reversal behavior. However, when the applied field is 48° relative to the [001] orientation [Fig. 3(b)], H_{ex} decreases with temperature instead, and with no springlike reversal [Fig. 3(a)]. In this case, magnetocrystalline anisotropy can force the AFM spins to align away from FM spins because of fewer thermal fluctuations, resulting in a weaker coupling.

V. CONCLUSION

In this paper, we have investigated the angle and temperature-dependent structural and magnetic properties of a V_2O_3/Py heterostructure. An exchange bias appears at the onset of the V_2O_3 antiferromagnetic transition. The magnitude of the exchange bias is more prominent for a field applied along the [001] V_2O_3, consistent with the AFM spin configuration on the (110) surface. We have provided evidence of the existence of a magnetic coupling at the interface below the MIT. This opens the door to voltage-controlled magnetism by electrical manipulation of exchange bias, for example, by combining V_2O_3 resistive switching with the functional properties of magnetic thin films.

The data that support the findings of this study are available from the corresponding author upon reasonable request.

ACKNOWLEDGMENTS

Work was supported by U.S. Department of Energy (DOE), Office of Science, Grant No. DE-FG02-87ER45332 and ANID, CHILE, FONDECYT, Project No. 1211902.

R.e.H., A.C.B., and I.K.S. conceived the idea and designed the experiments. R.e.H. fabricated the samples. R.e.H., A.C.B., T.D.W., and J.L. performed the magnetic and structural measurements. R.e.H., F.T., A.C.B., and I.K. S. analyzed and interpreted the results. All authors participated in the discussion of the results and corrected the manuscript.

The authors have no conflicts to disclose.

[1] F. Hellman, A. Hoffmann, Y. Tserkovnyak, G. S. D. Beach, E. E. Fullerton, C. Leighton, A. H. MacDonald, D. C. Ralph, D. A. Arena, H. A. Dürr *et al.*, Interface-induced phenomena in magnetism, Rev. Mod. Phys. **89**, 025006 (2017).

[2] J. Nogues and I. K. Schuller, Exchange bias, J. Magn. Magn. Mater. **192**, 203 (1999).

[3] B. Negulescu, D. Lacour, F. Montaigne, A. Gerken, J. Paul, V. Spetter, J. Marien, C. Duret, and M. Hehn, Wide range and tunable linear magnetic tunnel junction sensor using two exchange pinned electrodes, Appl. Phys. Lett. **95**, 112502 (2009).

[4] B. G. Park, J. Wunderlich, X. Martí, V. Holý, Y. Kurosaki, M. Yamada, H. Yamamoto, A. Nishide, J. Hayakawa, H. Takahashi *et al.*, A spin-valve-like magnetoresistance of an antiferromagnet-based tunnel junction, Nat. Mater. **10**, 347 (2011).

[5] T. Gasi, A. K. Nayak, J. Winterlik, V. Ksenofontov, P. Adler, M. Nicklas, and C. Felser, Exchange-spring like magnetic behavior of the tetragonal Heusler compound Mn_2FeGa as a candidate for spin-transfer torque, Appl. Phys. Lett. **102**, 202402 (2013).

[6] J. de la Venta, S. Wang, T. Saerbeck, J. G. Ramírez, I. Valmianski, and I. K. Schuller, Coercivity enhancement in V_2O_3/Ni bilayers driven by nanoscale phase coexistence, Appl. Phys. Lett. **104**, 062410 (2014).

[7] J. de la Venta, S. Wang, J. G. Ramirez, and I. K. Schuller, Control of magnetism across metal to insulator transitions, Appl. Phys. Lett. **102**, 122404 (2013).

[8] J.-W. Xu, Y. Chen, N. M. Vargas, P. Salev, P. N. Lapa, J. Trastoy, J. Grollier, I. K. Schuller, and A. D. Kent, A quantum material spintronic resonator, Sci. Rep. **11**, 15082 (2021).

[9] M. Erekhinsky, J. de la Venta, and I. K. Schuller, Spin valve effect across the metal-insulator transition in V_2O_3, J. Appl. Phys. **114**, 143901 (2013).

[10] J. Kim, J. Cramer, K. Lee, D. Han, D. Go, P. Salev, P. N. Lapa, N. M. Vargas, I. K. Schuller, Y. Mokrousov *et al.*, Tuning spin-orbit torques across the phase transition in VO_2/NiFe heterostructure, Adv. Funct. Mater. **32**, 2111555 (2022).

[11] M. Gibert, P. Zubko, R. Scherwitzl, J. Íñiguez, and J.-M. Triscone, Exchange bias in $LaNiO_3$-$LaMnO_3$ superlattices, Nat. Mater. **11**, 195 (2012).

[12] N. A. Butakov, I. Valmianski, T. Lewi, C. Urban, Z. Ren, A. A. Mikhailovsky, S. D. Wilson, I. K. Schuller, and J. A. Schuller, Switchable plasmonic–dielectric resonators with metal–insulator transitions, ACS Photonics **5**, 371 (2017).

[13] V. Humbert, R. El Hage, G. Krieger, G. Sanchez-Santolino, A. Sander, S. Collin, J. Trastoy, J. Briatico, J. Santamaria, D. Preziosi *et al.*, An oxygen vacancy memristor ruled by electron correlations, Adv. Sci. (Weinheim, Ger.) **9**, e2201753 (2022).

[14] V. Rouco, R. El Hage, A. Sander, J. Grandal, K. Seurre, X. Palermo, J. Briatico, S. Collin, J. Trastoy, K. Bouzehouane *et al.*, Quasiparticle tunnel electroresistance in superconducting junctions, Nat. Commun. **11**, 658 (2020).

[15] K. Ignatova, E. B. Thorsteinsson, B. A. Jósteinsson, N. Strandqvist, C. Vantaraki, V. Kapaklis, A. Devishvili, G. K. Pálsson, and U. B. Arnalds, Reversible exchange bias in epitaxial V_2O_3/Ni hybrid magnetic heterostructures, J. Phys. Condens. Matter **34**, 495001 (2022).

[16] J. M. Díez, J. L. F. Cuñado, P. Lapa, R. Solís, I. Arnay, P. Pedraz, P. Perna, A. Bollero, R. Miranda, I. K. Schuller *et al.*, Interfacial exchange phenomena driven by ferromagnetic domains, Adv. Mater. Int. **9**, 2200331 (2022).

[17] Y. Kalcheim, A. Camjayi, J. del Valle, P. Salev, M. Rozenberg, and I. K. Schuller, Non-thermal resistive switching in mott insulator nanowires, Nat. Commun. **11**, 2985 (2020).

[18] E. Qiu, Y. Zhang, M. Di Ventra, and I. K. Schuller, Reconfigurable cascaded thermal neuristors for neuromorphic computing, Adv. Mater. **36**, 2306818 (2023).

[19] P. Salev, J. del Valle, Y. Kalcheim, and I. K. Schuller, Giant nonvolatile resistive switching in a mott oxide and ferroelectric hybrid, Proc. Natl. Acad. Sci. USA **116**, 8798 (2019).

[20] J. Trastoy, Y. Kalcheim, J. del Valle, I. Valmianski, and I. K. Schuller, Enhanced metal–insulator transition in V_2O_3 by thermal quenching after growth, J. Mater. Sci. **53**, 9131 (2018).

[21] A. Glavic and M. Bjorck, GenX 3: The latest generation of an established tool, J. Appl. Crystallogr. **55**, 1063 (2022).

[22] Y. Kalcheim, C. Adda, P. Salev, M. Lee, N. Ghazikhanian, N. M. Vargas, J. del Valle, and I. K. Schuller, Structural manipulation of phase transitions by self-induced strain in geometrically confined thin films, Adv. Funct. Mater. **30**, 2005939 (2020).

[23] D. A. Gilbert, J. G. Ramírez, T. Saerbeck, J. Trastoy, I. K. Schuller, K. Liu, and J. de la Venta, Growth-induced in-plane uniaxial anisotropy in V_2O_3/Ni Films, Sci. Rep. **7**, 13471 (2017).

[24] J. G. Ramírez, J. de la Venta, S. Wang, T. Saerbeck, A. C. Basaran, X. Batlle, and I. K. Schuller, Collective mode splitting in hybrid heterostructures, Phys. Rev. B **93**, 214113 (2016).

[25] C. T. Wolowiec, J. G. Ramírez, M.-H. Lee, N. Ghazikhanian, N. M. Vargas, A. C. Basaran, P. Salev, and I. K. Schuller, Stress-tailoring magnetic anisotropy of V_2O_3/Ni bilayers, Phys. Rev. Mater. **6**, 064408 (2022).

[26] See Supplemental Material at http://link.aps.org/supplemental/10.1103/PhysRevMaterials.8.054407 for schematic representation of the AFM spin arrangements at the (110) V_2O_3 surface; magnetic measurement comparison between samples with and without breaking vacuum; discussion on the AFM grain and domain size in V_2O_3 layer. The Supplemental Material also includes Refs. [6,23].

[27] R. M. Moon, Antiferromagnetism in V_2O_3, Phys. Rev. Lett. **25**. 527 (1970).

[28] R. Tran, X.-G. Li, S. P. Ong, Y. Kalcheim, and I. K. Schuller, Metal-insulator transition in V_2O_3 with intrinsic defects, Phys. Rev. B **103**, 075134 (2021).

[29] B. S. Allimi, S. P. Alpay, D. Goberman, T. Huang, J. I. Budnick, D. M. Pease, and A. I. Frenkel, Growth of V_2O_3 thin films on *a*-plane (110) and *c*-plane (001) sapphire via pulsed-laser deposition, J. Mater. Res. **22**, 2825 (2007).

[30] A. P. Malozemoff, Random-field model of exchange anisotropy at rough ferromagnetic-antiferromagnetic interfaces, Phys. Rev. B **35**, 3679 (1987).

[31] A. P. Malozemoff, Heisenberg-to-Ising crossover in a random-field model with uniaxial anisotropy, Phys. Rev. B **37**, 7673 (1988).

[32] R. Morales, A. C. Basaran, J. E. Villegas, D. Navas, N. Soriano, B. Mora, C. Redondo, X. Batlle, and I. K. Schuller, Exchange-bias phenomenon: The role of the ferromagnetic spin structure, Phys. Rev. Lett. **114**, 097202 (2015).

[33] M. Kiwi, J. Mejía-López, R. D. Portugal, and R. Ramírez, Exchange-bias systems with compensated interfaces, Appl. Phys. Lett. **75**, 3995 (1999).